Experimental Determination of the $H_2SO_4/(NH_4)_2SO_4/H_2O$ Phase Diagram

Keith D. Beyer,* Jameson R. Bothe, and Nicola Burrmann

Department of Chemistry, University of Wisconsin—La Crosse, La Crosse, Wisconsin 54601

Received: July 18, 2006; In Final Form: November 11, 2006

We have experimentally investigated the water and sulfuric acid-rich regions of the $H_2SO_4/(NH_4)_2SO_4/H_2O$ ternary liquid/solid phase diagram using differential scanning calorimetry (DSC) and infrared spectroscopy of thin films. We present the liquid/solid ternary phase diagram for temperatures below 373 K and H_2SO_4 concentrations below 60 wt %. We have determined two ternary eutectics and two tributary reaction points for this system in the regions studied. It is also seen that sulfuric acid tetrahydrate (SAT) forms as a metastable solid over a large concentration range. Two true binary systems have been identified: ice/letovicite and SAT/ammonium bisulfate. Finally, we have compared our results to the predictions of the aerosol inorganics model and have found significant differences both in the final melting points and in the location of some of the phase boundaries including a significant discrepancy in the invariant points predicted versus those observed.

Introduction

Tropospheric aerosols are made up predominantly of aqueous ammonium and sulfate ions with the molar ratio of NH_4^+/SO_4^{2-} ranging from 0 to 2.[1,2] Observations during the subsonic aircraft: contrail and cloud effects special study (SUCCESS) revealed free tropospheric aerosols containing significant amounts of NH_4^+ and SO_4^{2-} including conditions where cirrus ice was present.[3] Also, theoretical studies have shown the importance of ammoniated sulfate aerosols in cirrus cloud formation.[4,5] These particles absorb and scatter solar radiation dependent upon their phase, thus contributing to the radiation balance.[6] They may also play a significant role in heterogeneous chemistry in the troposphere.[7] In all of these cases, understanding the thermodynamic properties at low temperatures is critical to knowing which phases may be present when particles crystallize and at what temperatures. Therefore, the thermodynamics of these systems needs to be studied to better understand tropospheric aerosols, aerosol chemistry, and cloud formation mechanisms.

The phase diagram of the $H_2SO_4/(NH_4)_2SO_4/H_2O$ ternary system has been little studied; it has been constructed from solubility data at room temperatures only.[8,9,10] Much low-temperature research has focused on the NH_4HSO_4/H_2O subsystem. We have studied this system in detail also, and our results are reported separately.[11] However, tropospheric aerosols may have a wide range of composition of NH_4^+/SO_4^{2-} ions, and thus, the NH_4HSO_4/H_2O system represents only a narrow range of possible aerosol compositions within the ternary $H_2SO_4/(NH_4)_2SO_4/H_2O$ system. Though Yao et al.[12] have calculated phase transition temperatures for the regions of the ternary phase diagram where ice may form, a thorough experimental determination of the solid/liquid phase diagram of this system as a function of composition and temperature has not been undertaken. In particular, solids may form in the concentration range where ice is stable that we are currently unaware of; the calculations of Yao et al. are only for known phases of the composite binary systems. However, even in this case, consideration of sulfuric acid octahydrate was omitted. These factors necessitate further study of the thermodynamics of this ternary system.

To study ternary systems, one must know the binary systems that compose the ternary system well in order to effectively identify solids that may form. Additionally, ternary solids may form, which then makes knowledge of the stable binary solids extremely important in order to discern between known and new solids. Beyer et al.[13] conducted a thorough study of the H_2SO_4/H_2O phase diagram, especially focusing on the region where ice is stable, and have determined the thermodynamic stability region for sulfuric acid octahydrate in detail. The binary phase diagram of $H_2SO_4/(NH_4)_2SO_4$ has also been measured[14] as well as limited work on the $(NH_4)_2SO_4/NH_4HSO_4$ binary system melting points.[15] Finally, the phase diagram of $(NH_4)_2SO_4/H_2O$ has been studied.[16,17] We present here our results for the phase diagram of $H_2SO_4/(NH_4)_2SO_4/H_2O$ with comparison to literature data and the output of the aerosol inorganics model.[18]

Experimental Section

Sample Preparation. Ternary samples were prepared by diluting 98 wt % ACS reagent grade H_2SO_4 and 99.99 wt % ACS reagent grade $(NH_4)_2SO_4$ supplied by Fisher or Aldrich with Culligan purified water. Concentrated sulfuric acid was standardized by acid−base titration. The concentration of all samples is known to ±0.40 wt %.

Infrared Spectra. The sample cell used for infrared spectra is shown schematically and explained in detail in previous literature.[19] Briefly, a small drop of ternary solution was placed between two ZnSe windows, which were held in the center of an aluminum block by a threaded metal ring. Sample volumes were 1−2 μL. On each side of the aluminum block, a Pyrex cell was purged with dry nitrogen gas. KBr windows were placed on the end of each cell, sealed with o-rings, and held in place by metal clamps. Heat tape was wrapped around the purge cells to prevent condensation on the KBr windows. The sample was cooled by pouring liquid nitrogen into a circular aluminum cup attached to the top of the main cell. The cell block was warmed by resistive heaters connected to a temperature controller. Temperature was measured by a copper/constantan thermo-

* To whom correspondence should be addressed. E-mail: Beyer.Keit@uwlax.edu.

10.1021/jp0645465 CCC: $37.00
Published on Web 01/03/2007

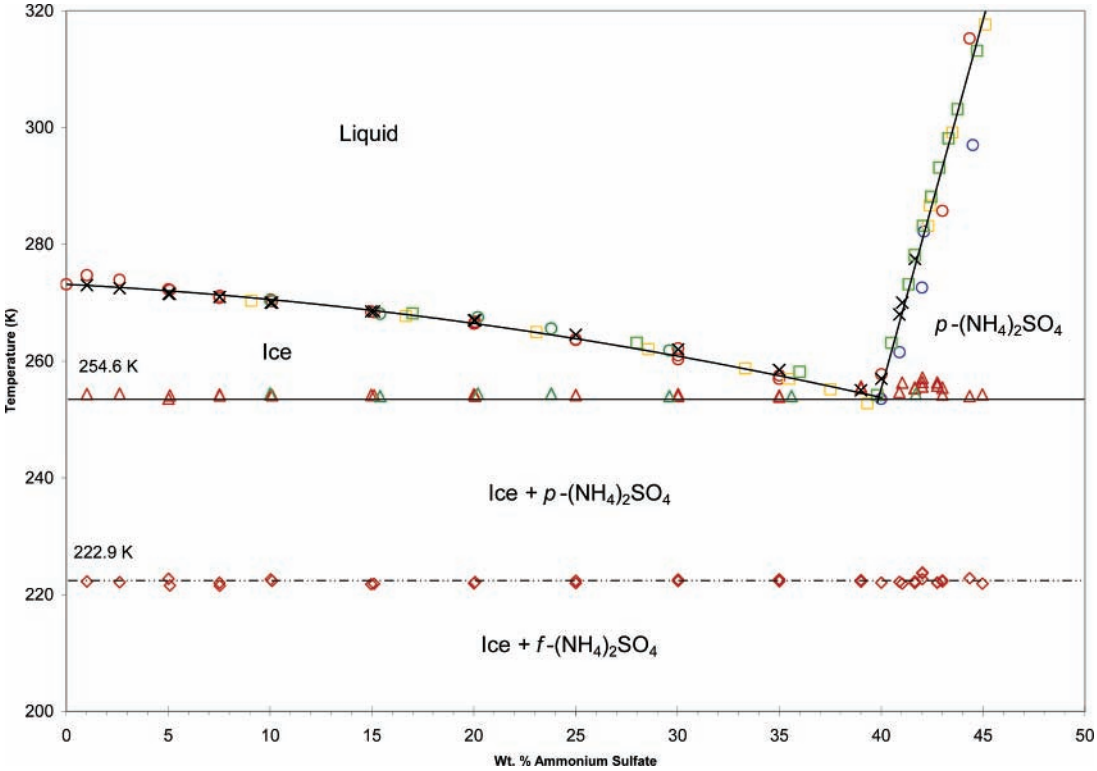

Figure 1. $(NH_4)_2SO_4/H_2O$ phase diagram; red symbols this work: circle, final melt/dissolution; triangles, eutectic melt; diamonds, ferro-electric solid/solid phase transition. Literature data: green symbols, Bertram et al.;[27] blue circles, Cziczo and Abbatt;[26] gold squares, Timmermans,[16] green squares, Linke.[17] Thermodynamic stability regions are labeled as follows: *p*-$(NH_4)_2SO_4$ = paraelectric phase of ammonium sulfate, *f*-$(NH_4)_2SO_4$ = ferroelectric phase of ammonium sulfate.

couple placed at the edge of the ZnSe windows and connected to the temperature controller. The temperature of the cell was calibrated using Culligan purified water and high purity organic solvents (Aldrich): decane, octane, and acetic anhydride of which the melting points are 243.5, 216.4, and 200.2 K, respectively.[20] The IR cell temperatures are known on average to within ±1.3 K; that is, a temperature we measured in the IR cell of a specific transition is within 1.3 K of the transition temperature we measure (of the same transition) using the DSC.

Spectra were obtained either with a Bruker Tensor 37 FTIR with an MCT−B detector at 8 cm^{-1} resolution (majority of samples) or a Mattson 4020 FTIR at 16 cm^{-1} resolution (minority of samples). Each spectrum is the average of 4 scans. Before spectra were taken of a sample, a background scan was obtained from a dry, purged sample cell. Samples were cooled to 192 K at 3 K/min and then allowed to warm to room temperature without resistive heating, typically this was 1 K/min. If samples did not freeze while cooling, they were held at 145 K for up to an hour and the samples would crystallize upon warming. In all cases, our spectra compare well for ice,[21] ammonium sulfate,[22] sulfuric acid tetrahydrate,[19] sulfuric acid hemihexa hydrate,[19] ammonium bisulfate,[23] and letovicite.[24]

Differential Scanning Calorimeter. Thermal data were obtained with a Mettler Toledo DSC 822e with liquid-nitrogen cooling utilizing both the FRS5 and HSS7 sensors. Industrial grade nitrogen gas was used as a purge gas with a flow rate of 50 mL/min. The temperature reproducibility of this instrument is better than ±0.05 K. Our accuracy is estimated to be ±0.9 K with a probability of 0.94 based on a four point temperature calibration[25] using indium, HPLC grade water, anhydrous, high purity (99%+) octane, and anhydrous, high purity heptane (99%+) from Aldrich, the latter three stored under nitrogen. The sensitivity of our instrument to thermal signals is high. Previously, we have calculated our sensitivity to detecting a component undergoing a thermal transition to be <50 ppm by mass using the FRS5 sensor. Tests in our lab have shown the HSS7 is about seven times more sensitive.

Samples were contained in a 30 μL platinum pan and typically had a mass of approximately 25 mg. In cases where samples did not freeze upon repeated runs, we used larger samples ranging from 60 to 120 mg contained in 70 or 150 μL platinum pans. Each sample was weighed before and after the experiment using a Mettler-Toledo AT20 microgram balance. The average mass loss from evaporation during the experiment was less than 1%. Samples with higher mass loss were not used in our evaluation. A typical sample was cooled to 138 K at 10 K/min, held at that temperature for 30 min, and warmed at a rate of 1 K/min to a temperature at least 5 K above the predicted melting point. In cases where samples did not completely freeze (especially at H_2SO_4 concentrations greater than 70 wt %), various other methods were attempted: holding at 183 K for 12 h, holding at 138 K for longer periods, holding at 190 K to attempt the induction of cold crystallization, and warming at 0.5 K/min. None of these methods were seen to induce complete freezing. All of our samples were cooled at 10 K/min. However, a few samples (six in different regions of the phase diagram) were cooled at 1 K/min to determine if there were influences on the number and types of phases that would crystallize. Our results show that an equal number or more phases crystallize utilizing slow cooling as compared to fast cooling.

Results

$(NH_4)_2SO_4/H_2O$. As a test case, we measured the phase diagram of $(NH_4)_2SO_4/H_2O$. The results are given in Figure 1 along with solubility data from the literature,[16,17] aerosol deliquescence experiments,[26] and emulsion data.[27] It is seen that there is excellent agreement among the data from disparate types

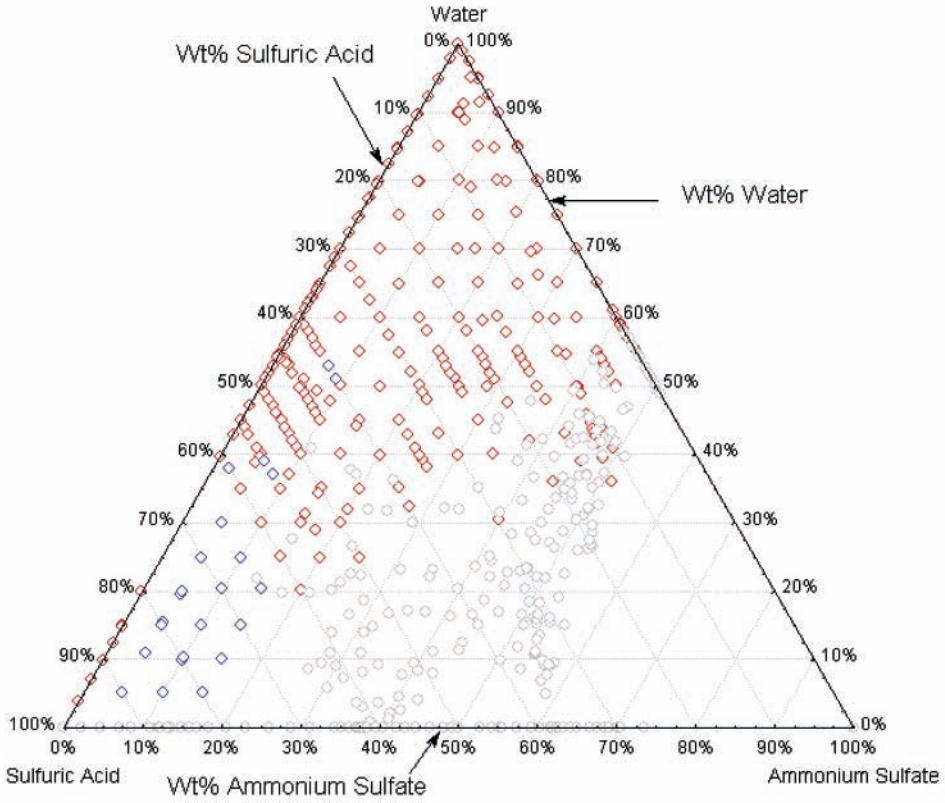

Figure 2. Ternary diagram for the $H_2SO_4/(NH_4)_2SO_4/H_2O$ system indicating concentrations studied in our lab and those given in the literature. Diamonds are concentration of samples run in our lab (red indicates the sample froze completely; blue, the sample did not freeze completely). Gray circles are literature data points from Silcock.[8] Concentrations on ternary phase diagrams in this paper are read in the following way: water concentrations are read horizontally using the scale on the right side of the diagram, H_2SO_4 concentrations are read 120° from horizontal using the scale on the left side of the diagram, $(NH_4)_2SO_4$ concentrations are read 240° from horizontal using the scale at the bottom of the diagram.

of experiments. We have also directly measured the enthalpy of the ferro-electric phase transition of $(NH_4)_2SO_4$.[28,29] The average enthalpy of all samples studied is 1.54 ± 0.39 kJ/mol for this transition. We also found excellent agreement in our IR experiments for the spectral changes due to the ferro-electric transition with those reported by Fortin et al.[30]

$H_2SO_4/(NH_4)_2SO_4/H_2O$. Figure 2 shows the concentration of the samples studied in our experiments along with the data points from the literature[8] that we used in our analysis. As seen in the figure, samples with $[H_2SO_4] < 61$ wt % generally froze completely. Samples with higher sulfuric acid concentration did not freeze completely even after long periods at low temperatures and large sample sizes. We studied 342 samples with concentrations given in Figure 2 (data from the H_2SO_4/H_2O binary system were reported in Beyer et al.[13]). Of these, 265 froze completely (red data points) as evidenced by the appearance of a melt at the ternary or binary eutectic.[31] Figure 3 shows the temperature contours and phase boundaries for this system based on an analysis of our data and solubilities from the literature. (For clarity we have plotted the solubility from Silcock between 273 and 373 K at 20 K intervals.) The complete set of experimental final melting/dissolution points for ternary samples are given in Table 1S in Supporting Information. (Note: throughout we refer to "melting" for ice and the sulfuric acid hydrates, and "dissolution" for the ammoniated salts for the temperature/composition at which the solid disappears into solution.) It should be noted that the data used to construct Figure 3 is not continuous but rather is at specific concentration intervals (in our studies every 5 wt % or less, in the solubility data[8] the concentration intervals vary). Therefore, the temperature contours are smoothed interpolations between data points and are only valid on the order of ±2 wt % for a given temperature. Boundary curve temperatures (the temperature at which two phases are in equilibrium) and compositions shown in Figure 3 were determined by plotting final melting/dissolution temperatures as a function of ammonium sulfate concentration while holding the sulfuric acid concentration constant. The melting/dissolution points were then fit to second-order polynomials on each side of the phase boundary and the resulting equations solved simultaneously for the phase boundary composition and temperature

$$T = A_2X^2 + A_1X + A_0 \quad (1)$$

where T is the melting/dissolution temperature in Kelvin, and X is the wt% of $(NH_4)_2SO_4$. The resulting phase boundary temperatures and compositions are listed in Table 1. A typical plot of this analysis is given for three cases in Figure 4. Coefficient values for the parametrizations in the respective primary phase fields are given in Table 2. The concentration ranges for which the equations are valid are also given in the table.

In the ice region, the parametrization reproduced our experimental melting/dissolution points to within ±1.0 K, which is essentially the same as our experimental accuracy of ±0.9 K, as described in the experimental section. Only two sulfuric acid concentration lines (35 and 40 wt %) passed through the SAH section. Here, our parametrization reproduced our melting points to within ±0.6 K. The concentration range 45−60 wt % H_2SO_4 covers the SAT region, and here our parametrization of the melting points reproduced our data to within ±0.9 K. Our parametrization of the data in the letovicite and ammonium

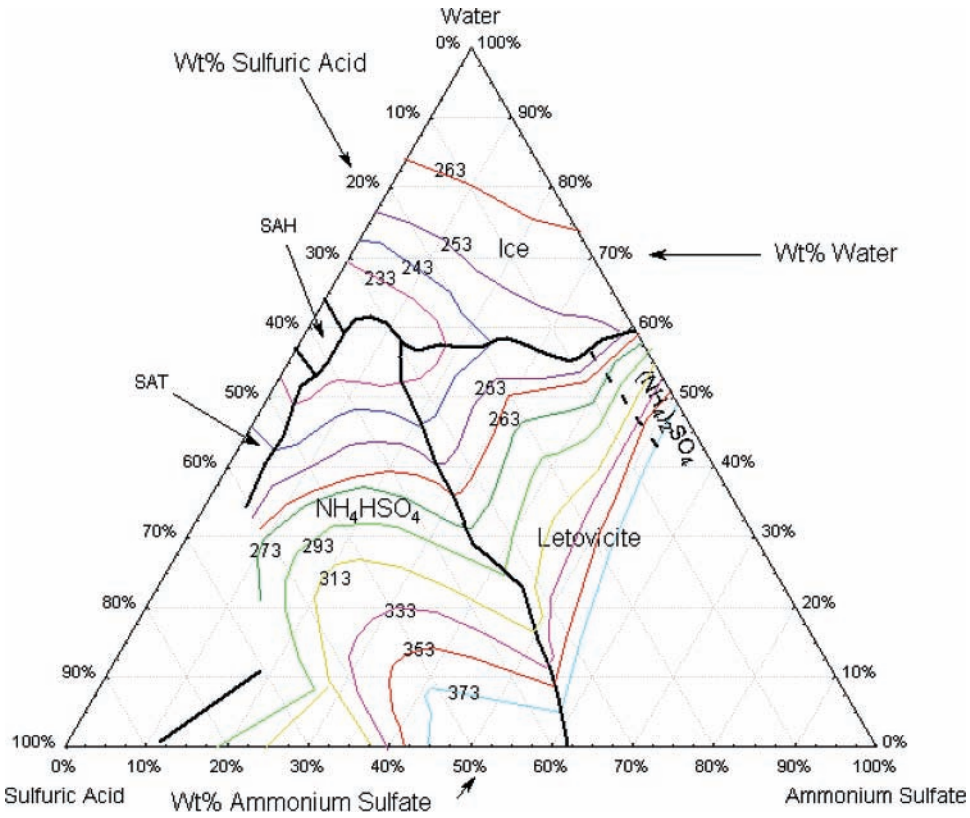

Figure 3. Results of our experimental studies coupled with solubility data from Silcock.[8] Black lines are phase boundaries (dashed line indicates a letovicite/ammonium sulfate phase boundary exists, but was not determined from our results or the literature solubility data). Colored lines are isotherms for the temperatures given on the diagram in Kelvin. Note, no data is available for the region in the lower left of the diagram (except at very high (>90 wt %) H_2SO_4 concentrations) or the lower right of the diagram.

TABLE 1: Phase Boundary Concentrations (wt %) and Temperatures as Determined from Our Experiments and Compared to the Predictions of AIM

			our data		aerosol inorganics model				
wt % SA[a]	wt% AS[a]	wt% H_2O	phase boundary temp. (K)	phase boundary solids[a]	initial transition temp. (K)	solid[a]	final transition temp. (K)	solid[a]	case[b]
5.0	37.0	58.0	250.6	Ice/AS	250.5	AS	250.5	Ice	A
8.8	35.5	55.7	247.6	Ice/Let	247.5	Ice	250.5	Let	1
10.0	35.0	55.0	249.3	Ice/Let	247.5	Ice	253.5	Let	4
15.0	27.0	58.0	246.0	Ice/Let	245.5	Let	246.0	Ice	A
15.6	25.0	59.4	245.4	Ice/Let	244.5	Let	247.0	Ice	4
17.9	24.1	58.0	244.6	Ice/Let	243.0	Ice	243.0	Let	5
20.0	22.8	57.2	239.5	Ice/Let	240.5	Ice	243.5	Let	2
25.0	17.0	58.0	231.7	Ice/Let	233.0	Ice	236.5	Let	2
28.3	15.0	56.7	226.9	Ice/Let	225.5	Ice	235.5	Let	4
30.0	8.2	61.8	218.0	Ice/ABS	220.5	Let	224.5	Ice	2
40.0	5.2	54.8	211.9	SAH/ABS	216.5	Let	217.0	SAH	6
45.0	3.4	51.6	227.6	SAT/ABS	218.0	SAH	227.5	SAT	3
50.0	5.1	44.9	239.0	SAT/ABS	231.5	ABS	238.0	SAT	3
55.0	4.2	40.8	245.1	SAT/ABS	242.5	ABS	243.0	SAT	5
60.0	5.1	34.9	240.3	SAT/ABS	240.5	SAT	253.5	ABS	1

[a] SA = H_2SO_4, AS = $(NH_4)_2SO_4$, Let = $(NH_4)_3H(SO_4)_2$, ABS = NH_4HSO_4, SAT = $H_2SO_4 \cdot 4H_2O$, SAH = $H_2SO_4 \cdot 6.5H_2O$. [b] Representative graphs of the comparison between our data and the AIM predictions are given in Figure 13 according to the specific case indicated in this column. A = AIM agrees with our data (within experimental error).

bisulfate primary phase fields performed significantly worse at reproducing the experimental dissolution points. Generally, we also included the solubility data from Silcock[8] in our parametrizations (unless we had enough experimental data points to establish a good correlation without the solubility data, see Figure 4 for examples). For letovicite and ammonium bisulfate regions, the parametrizations reproduced our data (and the included solubility data) to within ±2.4 and ±2.8 K, respectively.

We believe there are several reasons for the poorer performance of the parametrizations in these regions. First, the melting point and solubility data are more scattered than we observed in the ice, SAH, and SAT regions. This causes the parametrizations to be poorer fits to the data in the letovicite and ammonium bisulfate regions. Second, in the DSC experiments, we are attempting to detect the thermal signals of dissolution of NH_4HSO_4 and letovicite, which are very small. Ultimately, this leads to greater uncertainty in the final transition temper-

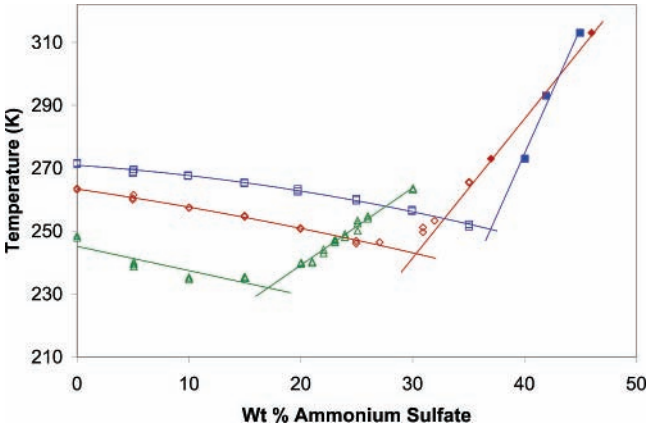

Figure 4. Plot of final melting/dissolution temperatures and concentrations of samples of 5 (blue), 15 (red), and 25 (green) wt % H_2SO_4, respectively. These are typical analyses which were performed for constant H_2SO_4 concentrations in the range of 5−60 wt % $(NH_4)_2SO_4$. Open symbols are our data, and solid symbols are solubility data from Silcock.[8]

TABLE 2: Melting/Dissolution Point Polynomial Coefficients from eq 1

$[H_2SO_4]$	A_2	A_1	A_0	valid $[(NH_4)_2SO_4]$
		Ice Primary Phase Region		
5	−0.00828	−0.244	270.9	0−37
10	−0.00424	−0.446	268.4	0−35
15	−0.00502	−0.526	263.3	0−27
20	0	−0.726	256.0	0−22.8
25	0	−0.806	245.3	0−16.3
30	0.156	−3.54	238.3	0−10.2
		SAH Primary Phase Region		
35	0	−2.24	216.0	0−5
40	0	−0.543	214.73	0−5.2
		SAT Primary Phase Region		
45	0	−0.0533	227.7	0−5
50	0	0.0492	238.8	0−5.1
55	0	−0.0307	245.3	0−4.2
60	0	−1.29	246.8	0−5.1
		Letovicite Primary Phase Region		
5	0	7.96	−43.7	37−45
10	0	8.64	−75.8	35−50
15	0	4.43	108.6	27−46
20	0	3.48	160.3	22.8−44
25	0	2.46	189.9	16.3−30
30	0.0274	1.004	207.9	10.2−45
		Ammonium Bisulfate Primary Phase Region		
35	0	1.9895	208.87	15−40
40	−0.146	7.06	179.1	5.2−25
45	0	2.83	217.6	5−30
50	0.131	0.846	231.3	5.1−22
55	0.133	1.19	237.8	4.2−20
60	−0.0507	5.69	212.6	5.1−22

atures than observed in the ice and hydrate regions. Third, in this region, a small change in concentration results in a large change in the salt dissolution temperature, since the temperature contours are very close together as seen in Figure 3. Because of these complications, and since we have demonstrated good agreement with literature data using our technique for the subsystems of this ternary (H_2SO_4/H_2O, $(NH_4)_2SO_4/H_2O$, and NH_4HSO_4/H_2O) here and in previous studies,[11,13] we did not specifically attempt to repeat the literature ternary solubility data. We have no data points that exactly match the concentration of solubility values from Silcock;[8] however, we have three data points that are within ±1 wt % of Silcock data points. Two are at 10% H_2SO_4, 40 and 45 wt % $(NH_4)_2SO_4$ where our dissolution temperatures were 1.85 K high and 6.99 K low, respectively, as compared to that of Silcock. Referring to Figure 3, it is seen that from 40 to 45 wt % $(NH_4)_2SO_4$ the solubility temperature changes 40 K, or 8 K for 1 wt % change in $(NH_4)_2SO_4$ concentration. (The change in the solubility temperature with respect to H_2SO_4 concentration is negligible in this region.) Given that the concentration of our samples and that of the literature data are within ±1 wt %, our temperature differences with the literature data are within the expected range. The third point is at 50.5/14.5 $H_2SO_4/(NH_4)_2SO_4$ where our datum is 10.32 K lower than Silcock. Here, the solubility changes 6 K for 1 wt % change in $(NH_4)_2SO_4$ concentration and 2 K for every 1 wt % change in H_2SO_4 concentration. We calculate that 8 K of the difference between our measured value and that of the literature is due to the uncertainty in our concentration measurements (±0.4 wt %) and the difference in the H_2SO_4 and $(NH_4)_2SO_4$ concentrations of our sample compared to the Silcock value. Thus, there is a 2.32 K difference between our measured value and that of Silcock beyond what can be explained by differences in concentration; however, the uncertainty in the Silcock data is unknown. We have four data points within 2 wt % of Silcock data. Three are within error limits based on differences in concentration (10.7/40 [two points] and 40.1/23.7 wt % $H_2SO_4/(NH_4)_2SO_4$), one (10.8/45.8 wt % $H_2SO_4/(NH_4)_2SO_4$) is 2.2 K beyond what can be explained due to differences and uncertainty in concentrations of our data compared to Silcock values. There are nine more data points that are within 2−8 wt % of Silcock data points. All of the differences in solubility temperatures between our data and that of Silcock can be explained by the differences in concentration of samples.

Alkemade Lines. Once the phase boundaries are known in a ternary system, Alkemade lines can be drawn between molecular solid compositions that share a phase boundary.[32] These Alkemades, which can be viewed as binary cross sections, constitute either a true or a pseudo-binary system. The Alkemade will be a true binary system if the Alkemade line intersects the common phase boundary between the binary solids. The Alkemade is a pseudo-binary if it does not intersect the common phase boundary between the binary solids. The binary subsystems are discussed individually in a section below (see "Binary Subsystems" section below for further discussion of an Alkemade system). Alkemade lines divide a ternary system into ternary "subsystems" which can be studied independent of the overall system. Alkemade lines for this system are given in Figure 5 (blue lines). Since these Alkemade subsystems constitute true ternary systems, each must have an invariant point: either within the Alkemade subsystem (a ternary eutectic) or outside the Alkemade subsystem (a tributary reaction point, discussed below).

Ternary Eutectics. The phase boundary analysis described above leads to the discovery of invariant points in the phase diagram. These points are labeled with capital letters in Figure 5 and identified in Table 3. Two ternary eutectics are identified: ice/$(NH_4)_2SO_4$/letovicite (point A in Figure 5) and ice/SAH/NH_4HSO_4 (point C in Figure 5). Because of the high temperature and weak thermal signals, we were unable to identify the letovicite/$(NH_4)_2SO_4$ phase boundary (dashed line in ternary phase diagram figures); therefore, we cannot identify the exact concentration of the ternary eutectic in the ice/$(NH_4)_2SO_4$/letovicite Alkemade region. However, we can set limits on the concentration based on our data for the phase boundaries: $[H_2SO_4] = 5.0-8.8$ wt %, $[(NH_4)_2SO_4] = 35.5-37.0$ wt %. The temperature is known from our data for all

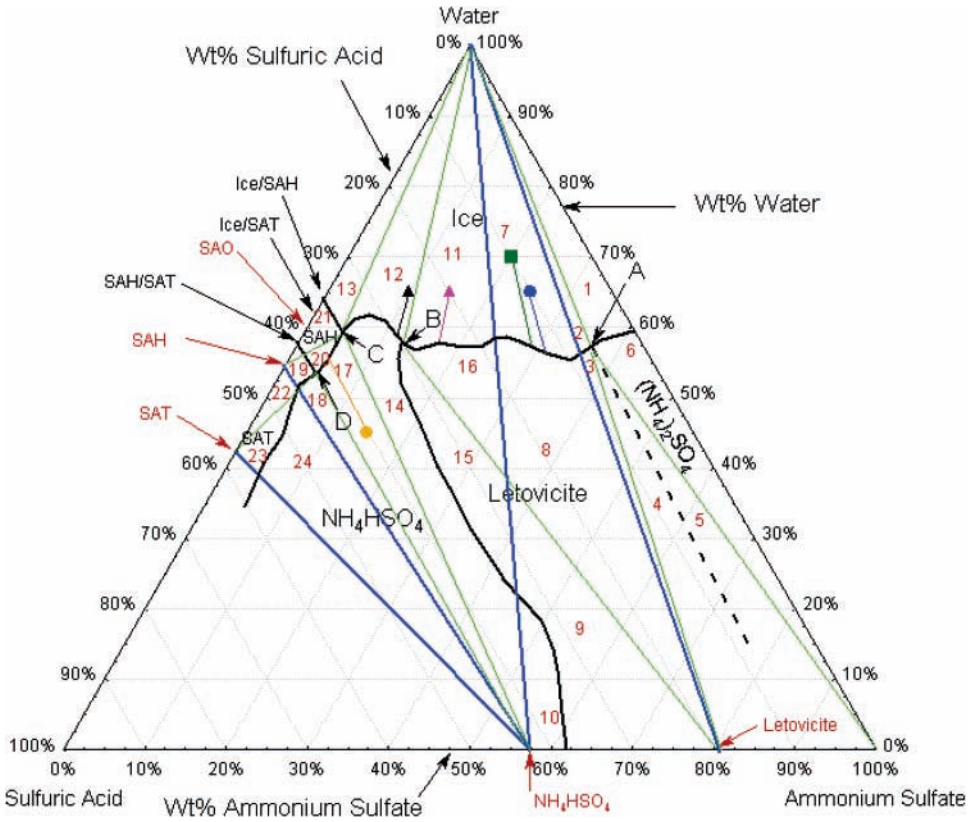

Figure 5. Ternary phase diagram showing phase boundaries (black lines) and Alkemade lines (blue). The Alkemade lines divide the ternary system into ternary subsystems. The ends of the Alkemade lines are molecular solids that share a phase boundary. The light green lines subdivide the Alkemade regions into regions of common melting order. Regions are numbered in red and explained in the text and in Tables 3 and 4. The four invariant points (zero degrees of freedom) are labeled with letters A−D. Colored points match thermograms given in Figure 6.

TABLE 3: Phase Diagram Invariant Points as Given in Figure 5

wt % H_2SO_4	wt % $(NH_4)_2SO_4$	T (K)	label in Figure 5	solids at invariant point	type of invariant point	Figure 5 regions terminating at this invariant point
5.0−8.8	35.5−37.0	247.6 ± 0.1	A	H_2O, $(NH_4)_2SO_4$, $(NH_4)_3H(SO_4)_2$	ternary eutectic	1−6
29 ± 1	12 ± 1	223.8 ± 0.8	B	H_2O, $(NH_4)_3H(SO_4)_2$, NH_4HSO_4	tributary reaction point	7−10
35 ± 2	5 ± 1	207.2 ± 0.3	C	H_2O, NH_4HSO_4, $H_2SO_4{\cdot}6.5H_2O$	ternary eutectic	11−21
42 ± 1	4 ± 1	218.1 ± 0.8	D	NH_4HSO_4, $H_2SO_4{\cdot}6.5H_2O$, $H_2SO_4{\cdot}4H_2O$	tributary reaction point	22−24

samples in the $H_2O/(NH_4)_2SO_4/(NH_4)_3H(SO_4)_2$ region that displayed a ternary eutectic transition (15 samples): 247.6 ± 0.1 K.

The ice/SAH/NH_4HSO_4 ternary eutectic is also problematic as it appears to fall very close to the H_2SO_4/H_2O binary, and few samples displayed this eutectic (14) in the ice/SAH/NH_4HSO_4 Alkemade region because SAH is very difficult to form, as was seen to be the case in the H_2SO_4/H_2O binary system.[13] However, the temperature of this eutectic can be determined from the average of the 14 samples: $T = 207.5 \pm 0.6$ K. Following the trend of final melting points in the region around point C in Figure 5, we estimate the ternary eutectic composition to be $[H_2SO_4] = 35 \pm 2$ wt%, $[(NH_4)_2SO_4] = 5 \pm 1$ wt%. The orange circle in Figure 5 represents a 40/15 wt % $H_2SO_4/(NH_4)_2SO_4$ sample, and the orange thermogram in Figure 6 shows the warming history. This is one of the few samples that displayed a signal due to SAH melting. In the thermogram, a large exotherm corresponding to the sample crystallization is seen at 190 K. The endotherm at 206.8 K is due to ice melting at the ice/SAH/NH_4HSO_4 ternary eutectic (point C in Figure 5). As warming continues, the phase boundary between SAH and NH_4HSO_4 is followed with continuous melting of both solids until 218.4 K where the last SAH melts. The liquid concentration then follows the orange tie line between the phase boundary and the total composition point (orange circle) as NH_4HSO_4 continuously dissolves until the final point of dissolution at 250.4 K. In the IR experiments, several of the 14 samples (that had an ice/SAH/NH_4HSO_4 endotherm in the DSC experiments) had very weak signals due to SAH in the ice primary phase region, mostly because of the very strong, interfering signal of ice. Also, samples closer to the SAH and NH_4HSO_4 primary phase regions have multiple overlapping peaks with SAT, NH_4HSO_4, and letovicite; however, a unique, noninterfering peak for SAH in this system appears to be 709 cm^{-1}.[19] The IR warming sequence for the 40/15 wt % $H_2SO_4/(NH_4)_2SO_4$ discussed above is given in Figure 7. At 192 K (blue spectrum), SAT, letovicite, and ice are present. At 195 K (red spectrum), SAT has melted as seen by the disappearance of the peak at 1060 cm^{-1} and the shoulder at 628 cm^{-1}. Simultaneously SAH has formed as given by the characteristic peak at 706 cm^{-1}. By 217 K (green spectrum), SAH has melted and the metastable letovicite has converted to NH_4HSO_4 as seen by the loss of the letovicite peak at 1130 cm^{-1} and the appearance of the characteristic NH_4HSO_4 peak at 913 cm^{-1}. Upon further warming, the NH_4HSO_4 continuously dissolves until dissolution has completed just before 252 K (black spectrum).

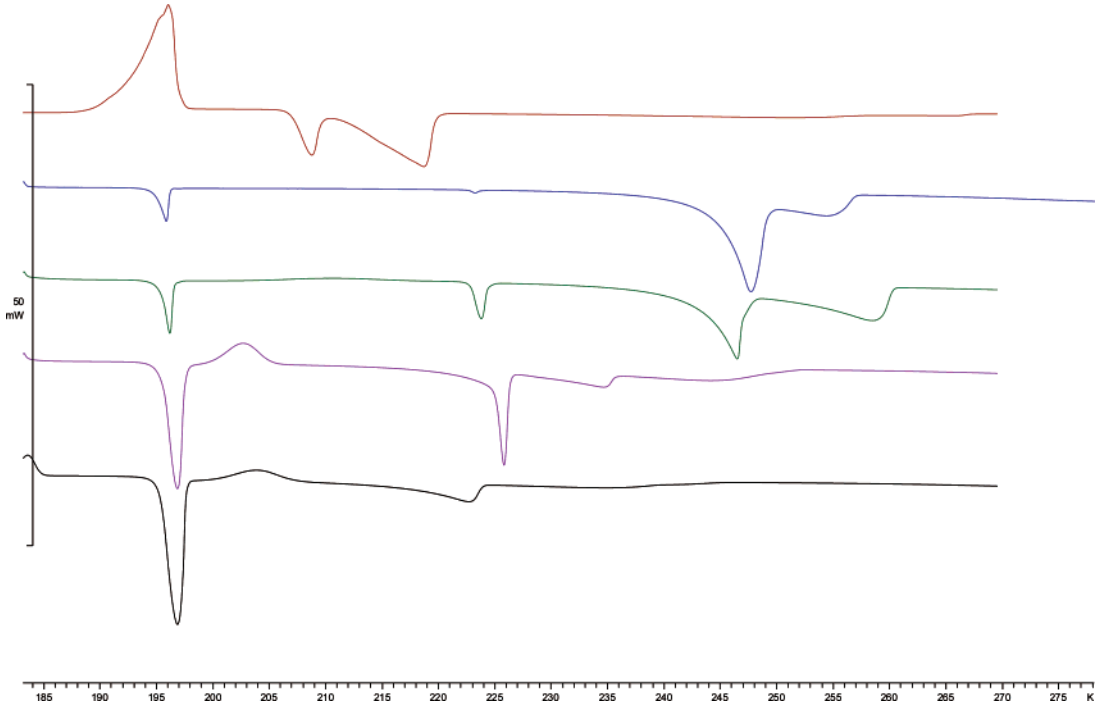

Figure 6. DSC thermograms for points marked in Figure 5; exotherms point up, and endotherms point down. Colors of thermograms correspond to colors of points in Figure 5 representing the concentration of each sample. The orange thermogram has been divided by three for ease of presentation and comparison.

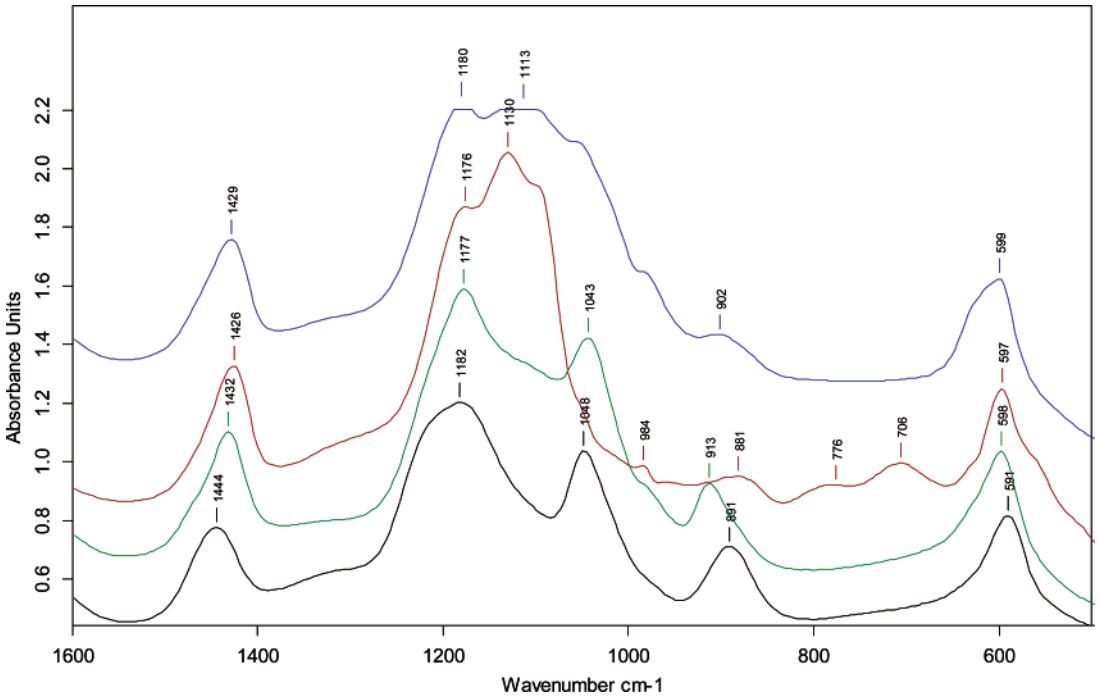

Figure 7. IR spectra of a 40/15 wt % $H_2SO_4/(NH_4)_2SO_4$ sample: blue (192 K) showing signature of SAT and letovicite with some ice, red (195 K) SAT has melted forming SAH, green (217 K) SAH has melted and letovicite has reacted to form NH_4HSO_4, and black (252 K) last NH_4HSO_4 has melted. Spectra are offset by the following for clarity: green, 0.1; red, 0.3; blue, 0.7 absorbance units.

Many samples that we studied in the $H_2SO_4/(NH_4)_2SO_4/H_2O$ phase diagram formed SAT (225 over all regions studied), including samples that displayed the stable ice/SAH/ammonium bisulfate ternary eutectic after recrystallization of the SAT melt (11 samples). However, the SAT primary phase field is relatively small, as is the Alkemade region where it would be thermodynamically stable (SAH/SAT/NH_4HSO_4 Alkemade triangle.) However, we observe SAT formation far outside this region (see section below on content of the solid phase). In all cases, SAT is observed to melt at 195.4 ± 1.0 K (average of all samples). We do not have enough data to definitively conclude whether this point is a metastable ternary eutectic involving SAT and other solids or simply a point of thermal decomposition of SAT. The shape of the thermograms leads us to conclude this transition point is likely the thermal decomposition of SAT, which in nearly all cases recrystallizes into other, stable solids. If the point were to be a ternary eutectic involving SAT, one would observe a significant slope to the baseline of the

thermogram upon further heating as the remaining two solids continuously melt along a phase boundary. We do not observe this to be the case in any of our samples. An example is given by the blue thermogram in Figure 6, which is a sample with concentration 10/25 wt % $H_2SO_4/(NH_4)_2SO_4$ (blue circle in Figure 5). The thermogram shows the SAT melt at 195 K followed by a very small endotherm we believe to be SAO melt. The small endotherm at 223 K is the dissolution of NH_4HSO_4 at point B, followed by the phase boundary dissolution of letovicite, and the final melt of ice at 248 and 254 K, respectively.

Tributary Reaction Points. Two other invariant points are apparent as a result of our analysis: tributary reaction points labeled B and D in Figure 5. It may be best to understand what occurs at these points from an equilibrium cooling perspective. Suppose a solution has a total concentration of $H_2SO_4/(NH_4)_2SO_4$ of 20/15 wt % as given by the purple triangle in Figure 5. Upon cooling, ice will begin to crystallize (at equilibrium) when the surface of the ice primary phase field is reached. Once ice forms, the concentration of the remaining liquid will move directly away from the ice apex and will follow the purple line in Figure 5 until the ice/letovicite phase boundary is reached. Upon further cooling, ice and letovicite continuously crystallize until point B is reached, where ammonium bisulfate begins to form. At this point, the degrees of freedom are zero since there are now three solids and one liquid in coexistence. However, our starting concentration falls within the ice/NH_4HSO_4/SAH Alkemade region; therefore, the final, completely solid sample must contain the Alkemade solids at equilibrium; hence, crystallization does not terminate at this invariant point. As NH_4HSO_4 is produced at point B, some letovicite is consumed

$$(NH_4)_3H(SO_4)_3\,(s) + H_2SO_4\,(aq) \rightarrow 3\,NH_4HSO_4\,(s) \quad (2)$$

However, in this system, letovicite is the limiting reagent in eq 2. Thus, once the conversion of letovicite to ammonium bisulfate is complete, a degree of freedom is restored, and the concentration of the liquid follows the ice/ammonium bisulfate phase boundary as these two solids continually crystallize upon further cooling. Finally, point C is reached where SAH forms and the final liquid is consumed as heat is removed. However, it should be noted that SAH is very difficult to form in this system, and thus the meta-stable SAT is more readily formed. If this is the case, samples will not completely freeze at point C but rather will freeze at some other point at a lower temperature, likely near point C in concentration, where SAT is formed. The order of events is reversed for a completely frozen sample as it is being warmed from below the temperature of the respective invariant point through the final melting of the last solid. The purple thermogram in Figure 6 shows the warming history of such a sample at the concentration of the purple triangle in Figure 5. First, SAT melts at 195 K, and a recrystallization of the melt ensues over the range 200−207 K which includes the conversion of any letovicite present into NH_4HSO_4, as confirmed in our IR experiments. Some ice and NH_4HSO_4 melts/dissolves along the phase boundary from point C to point B as indicated by the sloping baseline leading up to the endotherm at 224.8 K. At this point, the NH_4HSO_4 is converted to letovicite via the reverse of eq 2. Ice and letovicite melt/dissolve along the phase boundary until the point where the purple line in Figure 5 intersects the ice/letovicite phase boundary. At this point, the last letovicite dissolves at 234.5 K. Ice then continuously melts until the liquid reaches the concentration at the purple triangle where the last ice melts at 243.7 K. Point B is considered a tributary reaction point because two phase boundaries meet (ice/letovicite and letovicite/ammonium bisulfate) with a third phase boundary (ice/ammonium bisulfate) approaching from a lower temperature than either of the other two. Thus, the invariant point is not a temperature minima and some liquid remains upon further cooling in the example given, but one solid is eliminated, thus restoring a degree of freedom allowing composition to change upon further cooling. The conversion of one solid into another results in a "reaction" at the invariant point. This point occurs at $T = 223.8 \pm 0.8$ K (81 samples) and $[H_2SO_4] = 29 \pm 1$ wt %, $[(NH_4)_2SO_4] = 12 \pm 1$ wt %.

An alternative series of events occurs when the initial liquid composition is slightly different from that described above. Consider the composition $H_2SO_4/(NH_4)_2SO_4$ of 10/20 wt % represented by the green square in Figure 5. This composition lies in the ice/letovicite/ammonium bisulfate Alkemade region, and thus, the completely frozen sample must contain these three solids at equilibrium. The series of events of equilibrium cooling is the same as given above with the exception that more ice and letovicite are produced moving along the phase boundary. When the invariant point B is reached, again, the conversion of letovicite to ammonium bisulfate as given by eq 2 occurs. However, the key difference in this sample is that water and sulfuric acid are in shorter supply as more of each were used in forming ice and letovicite along the phase boundary than in the previous example. The result is that H_2SO_4 ends up being the limiting reagent in eq 2 for this sample, and when the reaction is complete, there is excess letovicite. The water has also been consumed forming the last bit of ice, thus eliminating the liquid phase. No further conversion can now occur as temperature is lowered; thus, point B becomes the terminus point for all solutions in the ice/letovicite/ammonium bisulfate Alkemade region. This path is also followed by samples whose concentration falls exactly on the ice/ammonium bisulfate alkemade line. In this special case, the terminus is still point B; however, there is exactly enough H_2SO_4 liquid for the complete conversion of letovicite to NH_4HSO_4 at point B. Thus only ice and solid NH_4HSO_4 remain at point B as shown by Beyer and Bothe.[11] Like the example given above, the order of events is reversed for a completely frozen sample as it is being warmed from below the respective invariant point through the final melting of the last solid. The melting sequence for this sample is illustrated by the green thermogram in Figure 6. In the thermogram, it is seen that SAT melts at 195 K followed by a broad recrystallization from 207 to 217 K. No appreciable slope to the baseline is seen leading to the tributary reaction point (endotherm) at 223 K, indicating liquid is not present. After NH_4HSO_4 is eliminated at the tributary reaction point, ice and letovicite continuously melt/dissolve as the liquid composition follows the phase boundary until the final dissolution of letovicite at 246 K (intersection of green tie line with the phase boundary in Figure 5). The liquid composition follows the green tie line until the final melt of ice at 258 K (green square).

Finally, if we consider a sample more acidified, with a concentration of 25/10 wt % $H_2SO_4/(NH_4)_2SO_4$, the invariant point B is not reached upon warming, and thus, the conversion of $NH_4HSO_4 \rightarrow$ letovicite does not occur at 224 K. The concentration of this sample is located at the black triangle in Figure 5, and its melting history is shown by the black thermogram in Figure 6. It is seen that SAT formed in this sample upon cooling and melts at 195 K. The melt is followed by a recrystallization at 198.5 K. As temperature increases, the phase boundary connecting points C and B is followed. Along this phase boundary NH_4HSO_4 and ice continuously melt/

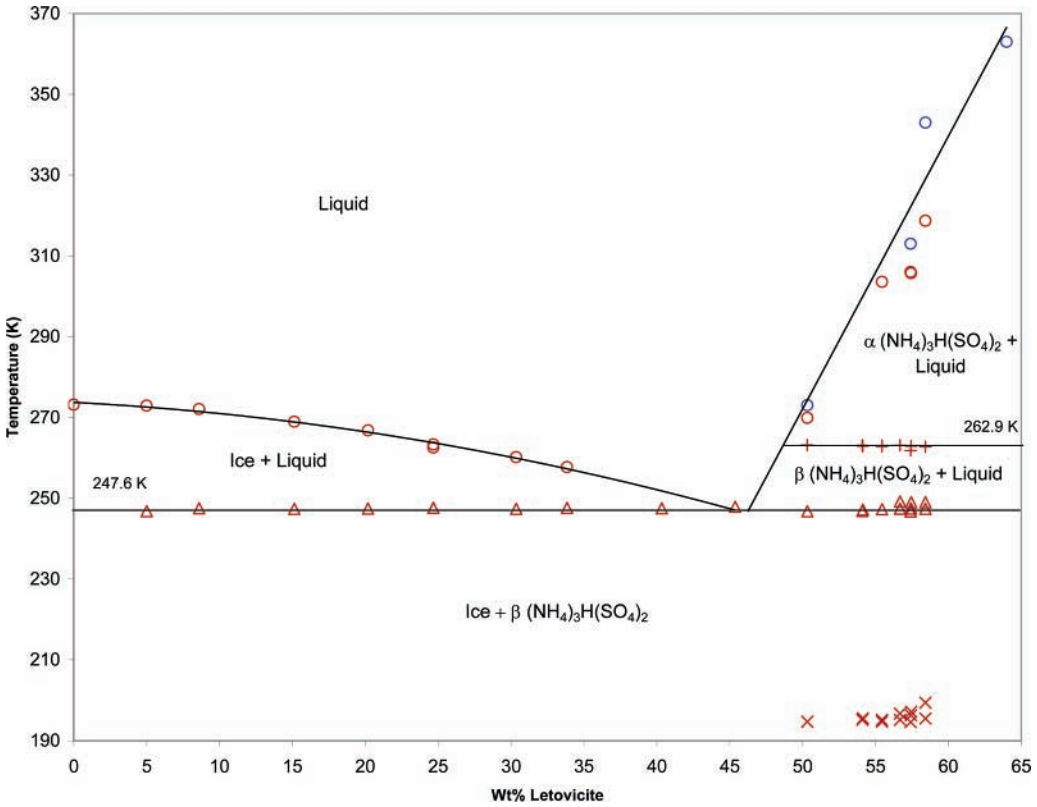

Figure 8. Ice/letovicite binary system phase diagram. Red symbols, this work: circles, final melt; triangles, eutectic melt; crosses, letovicite solid/solid phase transition; exes, SAT melt. Blue circles are data interpolated from Silcock[8] ternary system data.

dissolve until the point on the phase boundary where the tie line from the original concentration point (black triangle) intersects, 222.7 K. At this point, the last NH_4HSO_4 has dissolved and only ice remains. As temperature is increased further, ice continuously melts (following the black tie line) until the final melt point at 235.3 K (black triangle). As stated above, in contrast to the 20/15 wt % $H_2SO_4/(NH_4)_2SO_4$ sample, the 25/10 wt % $H_2SO_4/(NH_4)_2SO_4$ sample produces no letovicite as point B is never reached. Thus, the concentration of the liquid, even at equal water content, determines whether letovicite will be thermodynamically stable or not in a frozen sample.

The second tributary reaction point occurs at point D in Figure 5, where SAT is converted into SAH upon cooling at equilibrium. This invariant point also exists in the $H_2SO_4/HNO_3/H_2O$ system between SAT/SAH and nitric acid trihydrate (NAT).[33] Five samples appeared to display this transition, and we tentatively assign an invariant point temperature of 218.1 ± 0.8 K, with concentration at $[H_2SO_4] = 42 \pm 1$ wt %, $[(NH_4)_2SO_4] = 4 \pm 1$ wt %. Very few samples displayed this transition because SAH is very difficult to form and clearly detect under a wide range of conditions as discussed above, and we did not observe this transition in any of our IR experiments either because it did not appear or because the amount of solid in the SAH phase was below the instrument's detection limit. Therefore, we cannot confirm the identity of the solids involved in this transition detected in the DSC experiments.

Binary Subsystems. As seen in Figure 5, Alkemade lines exist between ice/letovicite, ice/NH_4HSO_4, NH_4HSO_4/SAH, and NH_4HSO_4/SAT (each of these binaries share a phase boundary). If the phase boundary between the two molecular solids that constitute the Alkemade intersects the Alkemade line, then the system is a true binary and follows the Gibbs phase rule. Both ice/letovicite and NH_4HSO_4/SAT Alkemade lines follow this rule. Thus, one would expect to observe a simple binary phase diagram for each of these. Figure 8 shows our DSC data for the H_2O/letovicite system, and Figure 9 shows typical thermograms for several concentrations. Clearly H_2O/letovicite displays the characteristics of a simple binary system as seen in the thermograms of Figure 9. In each case, the eutectic melt occurs at 250.2 ± 0.7 K with the final melt following at a higher temperature. These observations are confirmed in our IR experiments where we observed spectra characteristic of only ice and letovicite in the solid phase. We have no indication of ternary transitions occurring, except at the higher concentrations of letovicite where a small signal due to SAT melting is seen.

Although it is clear from Figure 5 that NH_4HSO_4/SAT constitutes a true binary system, we do not have enough experimental evidence to demonstrate this from DSC or IR data. It was difficult to get samples to completely freeze along this Alkemade, thus our data is incomplete. However, because the two primary phase fields share a phase boundary and the Alkemade line intersects it, thermodynamic theory states that this constitutes a true binary system.

When the phase boundary between two molecular solids that constitute the Alkemade does not intersect the Alkemade line, then the system is a pseudo-binary system, and generally violates the Gibbs phase rule over a finite concentration range when viewed as a binary system. Both ice/NH_4HSO_4 and NH_4HSO_4/SAH fall into this category as seen in Figure 5. Beyer and Bothe[11] performed a detailed study of the ice/NH_4HSO_4 system, demonstrating it is a pseudobinary. We do not have enough data for the NH_4HSO_4/SAH Alkemade to perform a similar study, since SAH is so difficult to form in this system.

Melting Order of Solids. As demonstrated above, the total composition of the sample determines which of the three solids must be present at equilibrium at a ternary eutectic or an invariant point. The identity of the three solids is given by which Alkemade region the total sample concentration lies in. One

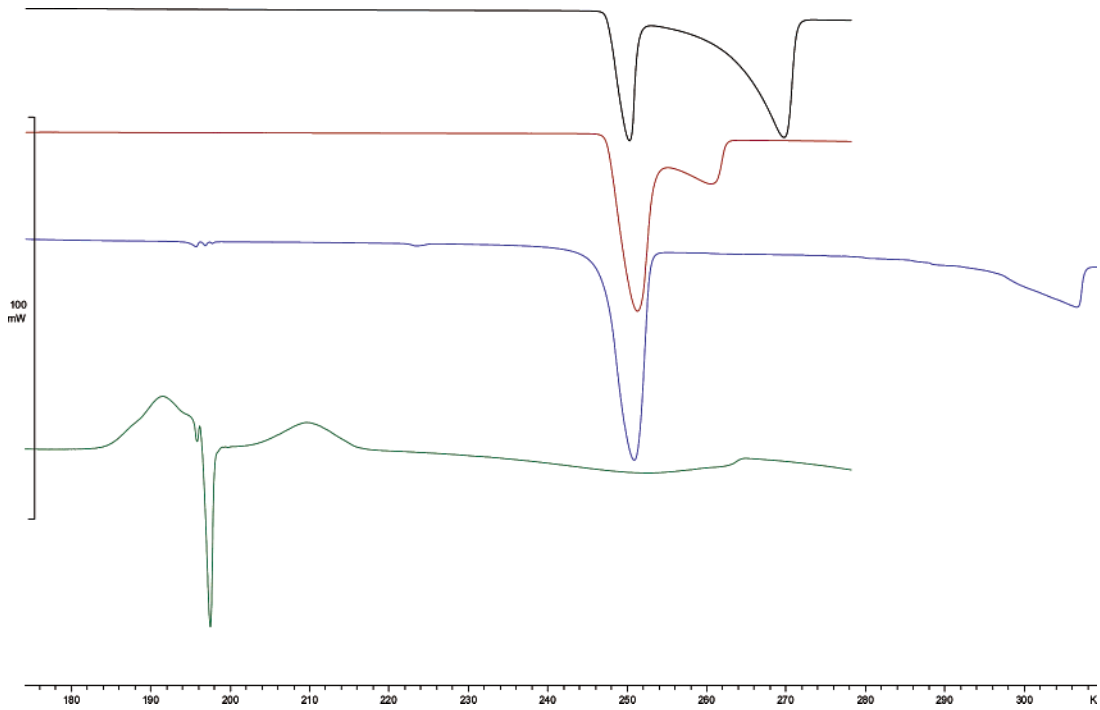

Figure 9. DSC thermograms for the ice/letovicite system showing true binary system behavior. Sample concentrations are as follows: black 15.1, red 30.4, and blue 57.4 wt % letovicite. The green thermogram is a sample of 35/20 wt % $H_2SO_4/(NH_4)_2SO_4$ illustrating the transitions for a sample in region 14 of the phase diagram in Figure 5 (see text). The thermogram has been multiplied by 8 for illustration purposes.

can then further divide the Alkemade regions into regions of common melting or freezing (at equilibrium) sequence upon warming or cooling. We have done this in Figure 5, and the regions are numbered 1 through 24 separated by green lines and the phase boundary curves. Examples of equilibrium freezing order were given above for several samples. First, using the sample concentration, one can determine the Alkemade region in which the sample lies. A completely frozen sample at equilibrium will be composed of the three solids that make up the Alkemade triangle. (The Alkemade lines themselves constitute binary systems, and a sample whose concentration lies directly on an Alkemade line will be composed only of the two solids that constitute the Alkemade line when completely crystallized at equilibrium.) Then, one can trace the equilibrium crystallization path: a line is drawn from the apex of the solid in whose primary phase field the total composition lies through the composition point to the phase field boundary. Equilibrium crystallization will then follow the phase boundary in the direction of lower temperature to the invariant point where the primary phase fields that constitute the original Alkemade region meet. One can then determine the order of melting phases by following the reverse path. A summary of the order of melting by region in Figure 5 is given in Table 4.

Content of the Solid Phase. The content of the solid phase can be determined from the fusion enthalpies of the various solids present. Mass fraction of each phase in a sample is calculated using the following equation:

$$y_i = \frac{EM_i}{\Delta H_i^{fus} m_T} \quad (3)$$

where y_i is the mass fraction of species i, E is the energy of the transition as measured by the DSC, M_i is the molar mass of solid i, ΔH_i^{fus} is the molar enthalpy of fusion of species i, and m_T is the total mass of the sample; where i represents ice and SAT and their respective fusion enthalpies are readily known.[34]

TABLE 4: Melting/Dissolution Order for Samples with Concentrations Lying in Regions Labeled in Figure 5

region of Figure 5	melting/dissolution order[a]
1	letovicite, $(NH_4)_2SO_4$, ice
2	$(NH_4)_2SO_4$, letovicite, ice
3	$(NH_4)_2SO_4$, ice, letovicite
4	ice, $(NH_4)_2SO_4$, letovicite
5	ice, letovicite, $(NH_4)_2SO_4$
6	letovicite, ice, $(NH_4)_2SO_4$
7	NH_4HSO_4, letovicite, ice
8	NH_4HSO_4, ice, letovicite
9	ice, NH_4HSO_4, letovicite
10	ice, letovicite, NH_4HSO_4
11	SAH, NH_4HSO_4 ($NH_4HSO_4 \rightarrow$ letovicite), letovicite, ice
12	SAH, NH_4HSO_4, ice
13	NH_4HSO_4, SAH, ice
14	SAH, ice, NH_4HSO_4
15	SAH, ice ($NH_4HSO_4 \rightarrow$ letovicite), NH_4HSO_4, letovicite
16	SAH, ice ($NH_4HSO_4 \rightarrow$ letovicite), ice, letovicite
17	ice, SAH, NH_4HSO_4
18	ice, SAH (SAH $\rightarrow$ SAT), SAT, NH_4HSO_4
19	ice, SAH (SAH $\rightarrow$ SAT), NH_4HSO_4, SAT
20	ice, NH_4HSO_4, SAH
21	NH_4HSO_4, ice, SAH
22	NH_4HSO_4, SAH, SAT
23	SAH, NH_4HSO_4, SAT
24	SAH, SAT, NH_4HSO_4

[a] In parentheses are the reactions that occur if the liquid passes through a tributary reaction point.

Few samples showed any indication of SAH content. Also, although thermal signals that we interpreted to be the melting of SAO were observed in many samples, the amount of SAO fell below our detection threshold in the IR experiments. Therefore, we were unable to quantify the amount of either SAH or SAO in the solid phase of our samples. Finally, it is known that ammoniated sulfates decompose before they reach a melting point,[35] and we were unable to determine their fusion enthalpies directly or indirectly in DSC experiments.

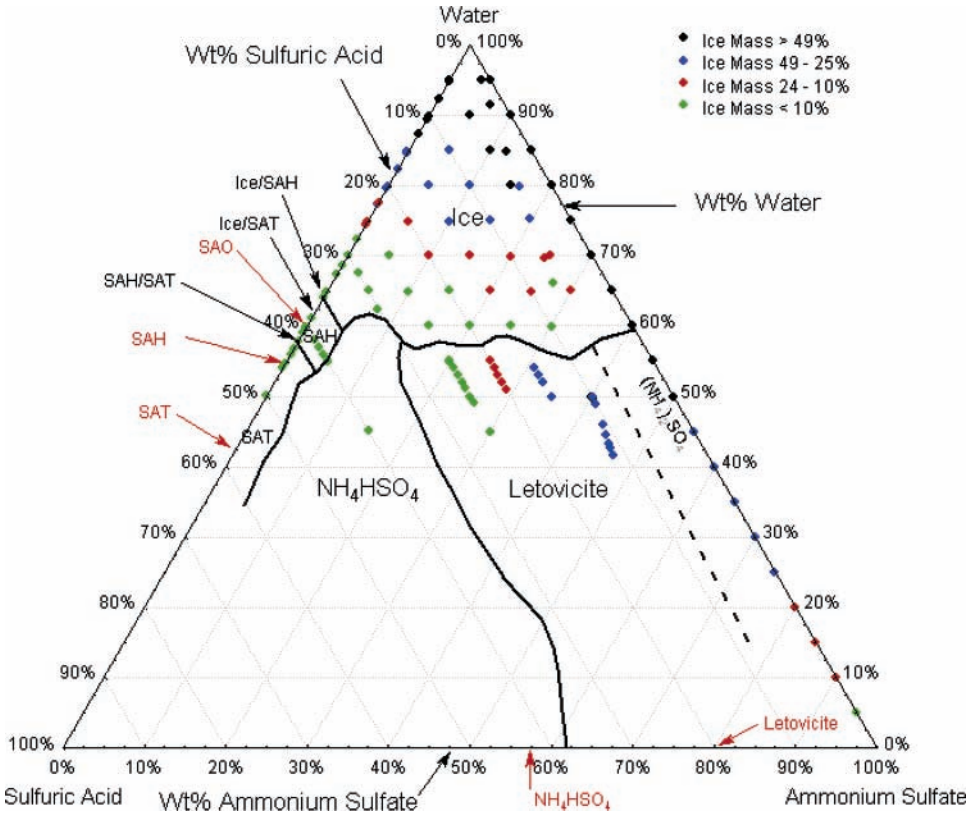

Figure 10. Fraction of frozen sample that is ice. Fractions represented by symbols in the diagram are given in the legend.

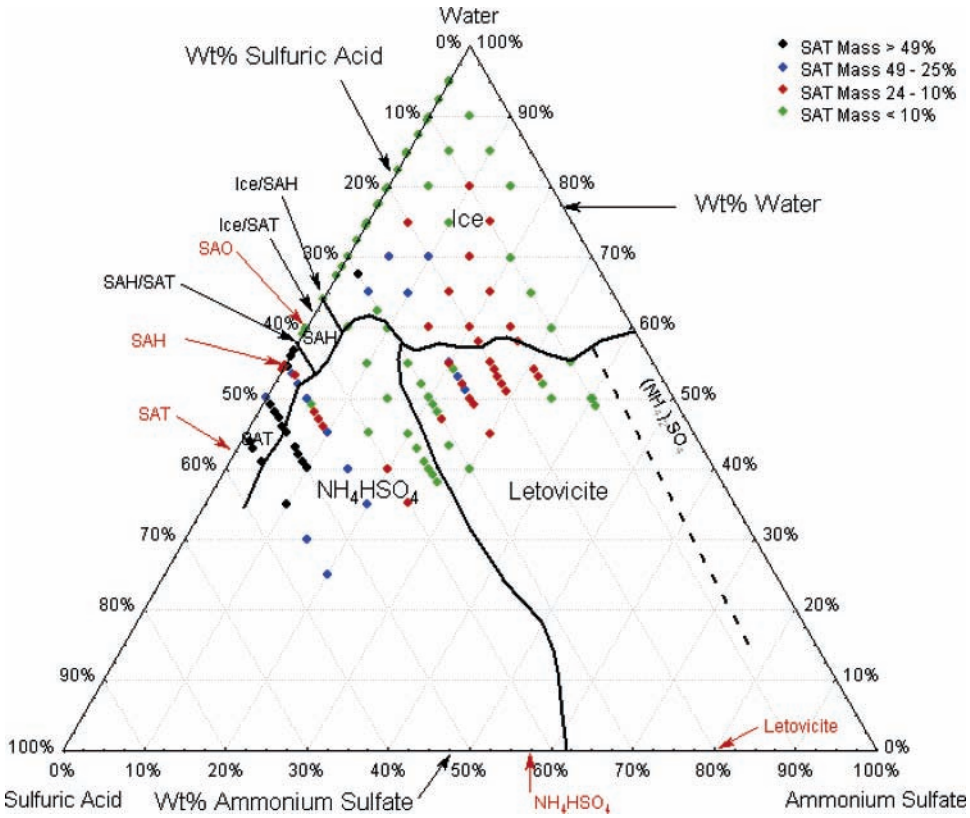

Figure 11. Fraction of frozen sample that is SAT. Fractions represented by symbols in the diagram are given in the legend.

We have determined the fraction by mass of samples that contained either ice or SAT. We then categorized the fractions by amount. The results are shown in Figures 10 and 11, respectively. For the ice fraction, it must be noted that, in almost all samples that displayed a SAT melt, a recrystallization followed. It is highly likely some of the liquid from the SAT melt crystallized to form ice. Referring to Figure 10, samples near the water apex form the largest fraction of ice upon freezing, as expected. However, what is unusual is the significant amount of ice formed at low H_2SO_4, high $(NH_4)_2SO_4$ concentra-

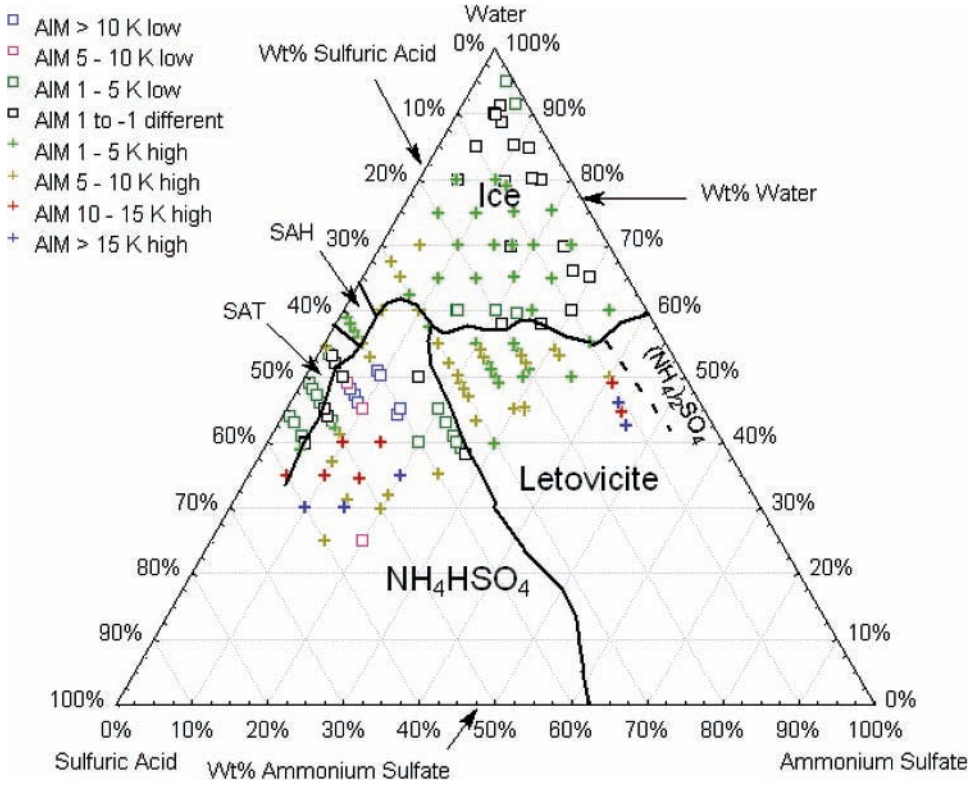

Figure 12. Difference between prediction of AIM model and our final melting/dissolution temperatures (AIM, our data) in K. Symbols are as given in the legend at the upper left.

tions. In this region ($[H_2SO_4] < 20$ wt %, $[(NH_4)_2SO_4] > 30$ wt %), ice remains a significant component of the frozen solid (25 − 50%), even though the total water content is low. Even at 20 wt % H_2SO_4, the ice fraction remains 10−24%. We reviewed all of these thermograms and found no anomaly in the data or unexpected artifacts that would have systematically skewed the data in this region. Since ice and the hydrates of sulfuric acid are the only solids with water content in this system, it would seem that our results indicate ice forms at the expense of SAT in this region. Probably, more of the H_2SO_4 in this region is tied up in letovicite (since this concentration range is in the letovicite primary phase field) than in the other regions. Thus, less SAT forms which frees water to form ice.

The SAT fraction (Figure 11) appears as expected. The SAT fraction is the highest in and close to the SAT primary phase field. However, there is still significant content well outside the SAT stability region or the SAH/SAT/NH_4HSO_4 Alkemade region. In these cases, it must be noted that a recrystallization almost always occurred after the SAT melt. It must also be noted that outside the SAH/SAT/NH_4HSO_4 Alkemade region SAT formation is metastable. Thus, its formation and mass fraction of the solid phase cannot be predicted using the lever rule. This leads us to conclude that SAT has a higher nucleation rate or crystal growth rate than competing solids in this system at temperatures below 195 K (SAT melting temperature). We also observe that the SAT fraction is somewhat lower for 30 and 35 wt % H_2SO_4 samples than what would be expected given the content observed for solutions of lower H_2SO_4 concentration. However, we observe that samples of 30 and 35 wt % H_2SO_4 had significant peaks due to (what we assigned to be) SAO melting, which would logically decrease the amount of SAT formed.

Comparison with AIM. We have compared our experimentally determined final melting points with those predicted by the aerosol inorganics model (AIM).[18] It must be noted that the AIM for this system is based on data sets between 273 and 323 K; therefore, predicting melting points and phase transitions below 273 K with the AIM is an extrapolation of the data on which the model is based. However, the web version (http://www.aim.env.uea.ac.uk/aim.html) allows temperatures between 180 and 330 K to be entered into the model for calculations.

The results of our analysis are given in Figure 12 and are categorized into temperature difference bins. The range in the difference between the AIM predictions and our dissolution temperatures is −15 to +20 K with an average (absolute value) difference of 5.3 K and a median (absolute value) of 4.1 K. We performed the same analysis using the solubility data from Silcock[8] for temperatures between 273 and 323 K and water concentrations greater than 10 wt %. We found the average (absolute value) difference between the Silcock data and the AIM predictions to be 5.5 K with a median (absolute value) difference of 2.0 K. Clegg et al.[18] plot the solubility data of Silcock used in the AIM with their fits to the data (AIM predictions) using the molality scale for concentration (see their Figure 20). It must be noted that small changes in molality can lead to large differences in solubility temperature because the salt solubilities change rapidly with temperature in much of the Silcock data.

When comparing the AIM predictions with our data, the AIM performs best near some of the phase boundaries. It is generally high by 1−10 K in the ice, letovicite, and SAH primary phase fields. It is low in the SAT region and the water-rich region of the NH_4HSO_4 primary phase field. However, it is high in the water poor area of the NH_4HSO_4 region. The discrepancies in the NH_4HSO_4 primary phase field in the final melt temperatures are most likely due to the differences between the letovicite/NH_4HSO_4 phase boundary predicted by AIM and that measured from our experiments. Also, as a general note, the accuracy of our dissolution temperatures is poorer in the letovicite and

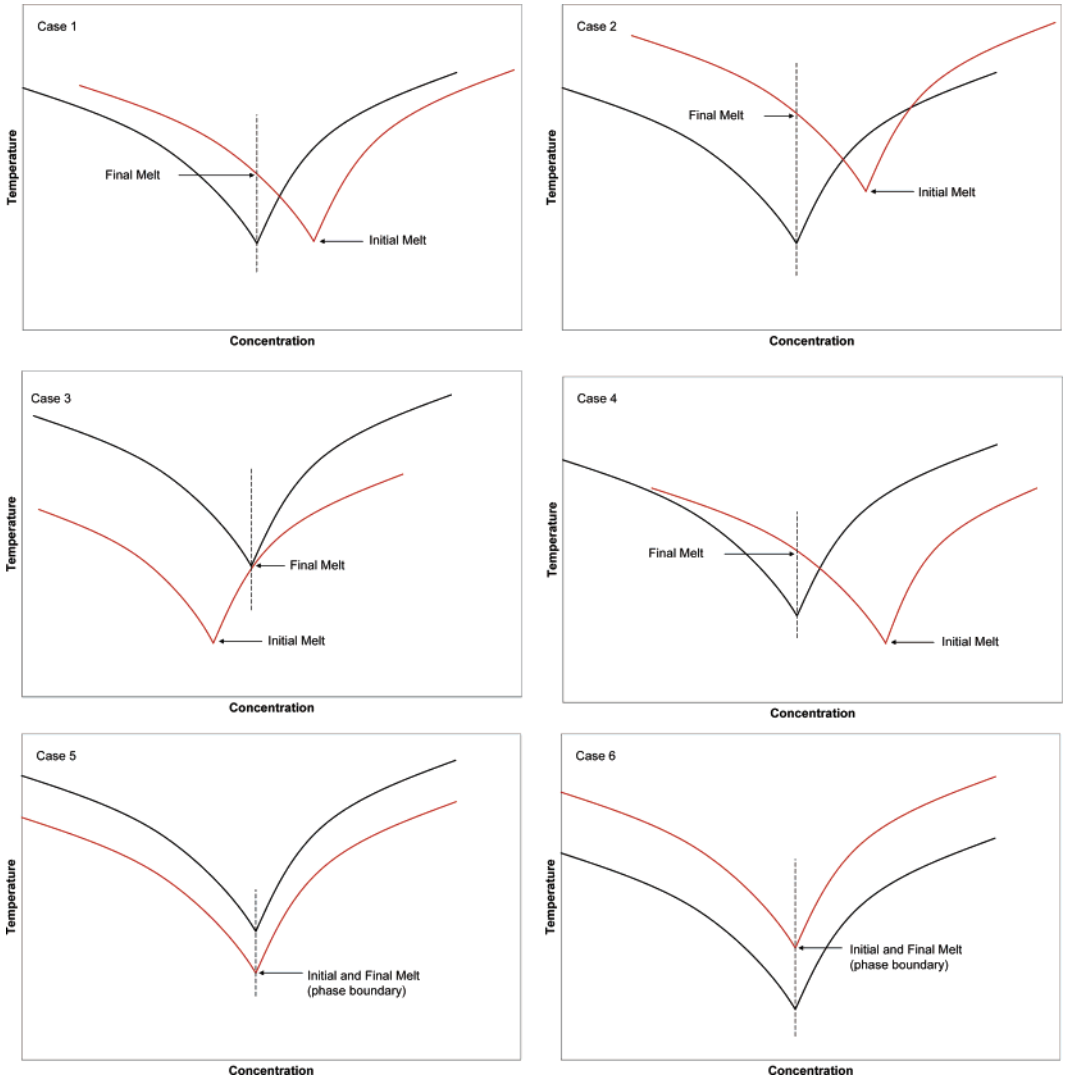

Figure 13. Visual representations of the differences between the experimentally determined phase boundaries (black curves) and those determined from the AIM (red curves). The concentration of the solution at the phase boundary from experiments is indicated by the dashed line. The arrows indicate the temperatures of the initial and final melts predicted by AIM for each case relative to the experimental phase boundary temperature. Case 1: AIM and experimental phase boundary temperatures are equal, but concentrations are not. Cases 2−4: AIM and experimental phase boundary temperatures and concentrations are not equal. Cases 5 and 6: AIM and experimental phase boundary concentrations are equal, but temperatures are not.

ammonium bisulfate primary phase fields. This is due to the observation that the dissolution enthalpies are very small, and the transition is spread over a large temperature range when the final dissolution is far from the phase boundary. Thus, the thermal signals tend to have a very small slope, and the assignment of final dissolution temperatures becomes difficult. See the final endotherm in the orange thermogram in Figure 6 as an example (40/15 wt % $H_2SO_4/(NH_4)_2SO_4$). It is seen that the largest discrepancies in dissolution temperatures between our data and that predicted by the AIM occur in the letovicite and ammonium bisulfate primary phase fields, especially far from the phase boundary.

We also compared the experimentally determined phase boundaries with those predicted by the AIM. In Table 1, we report our experimental phase boundary temperatures and compositions. We used our experimental compositions in the AIM to determine: the final melting temperature of the second phase (which we will call the "initial" melting temperature) and the final melting temperature of the final phase. If the AIM predicted the composition to be a phase boundary, the difference between the initial and final melting temperatures would be zero, as the solids would co-melt. Five compositions in Table 1 fall into this category. Second, if initial melting predicted by the AIM was to coincide with the experimental phase boundary, then the difference between the experimental temperature and that predicted by the AIM would be zero. In this latter case, it is seen that of the five phase boundaries predicted by AIM only two coincide in temperature with the experimentally determined phase boundary, as seen in Table 1. This leads to the observation that in some areas of the phase diagram, the AIM-predicted phase boundaries do not coincide with the experimentally determined phase boundaries. Generally, these differences fall into six cases, which are shown visually in Figure 13. Significant deviations between the two phase boundaries begin at water concentrations greater than about 35 wt %. In fact, the AIM predicts a $SAT/(NH_4)_3H(SO_4)_2/NH_4HSO_4$ ternary eutectic, whereas the analysis of our data reveals an $ice/(NH_4)_3H(SO_4)_2/NH_4HSO_4$ tributary reaction point as discussed above. The prediction of AIM leads to the conclusion that ice/NH_4HSO_4 cannot coexist at equilibrium (they do not share a phase boundary in the AIM prediction); however, our results and those given in detail by Beyer and Bothe[11] indicate this is not the

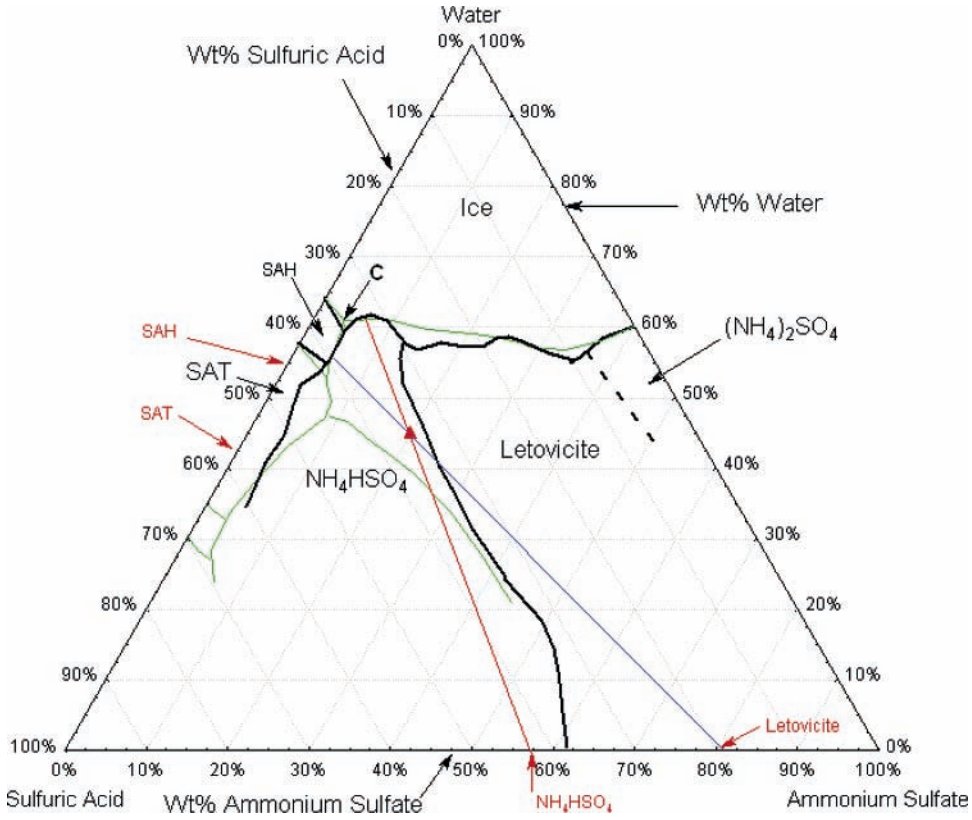

Figure 14. Comparison of our phase boundaries with those generated using AIM.[18] Black lines are experimentally determined phase boundaries from our results and literature solubility data.[8] Green lines are those generated from the AIM. Red triangle represents the concentration of the sample corresponding to the green thermogram in Figure 9. Red and blue lines are discussed in the text. Red text and arrows refer to the exact composition of the binary solids.

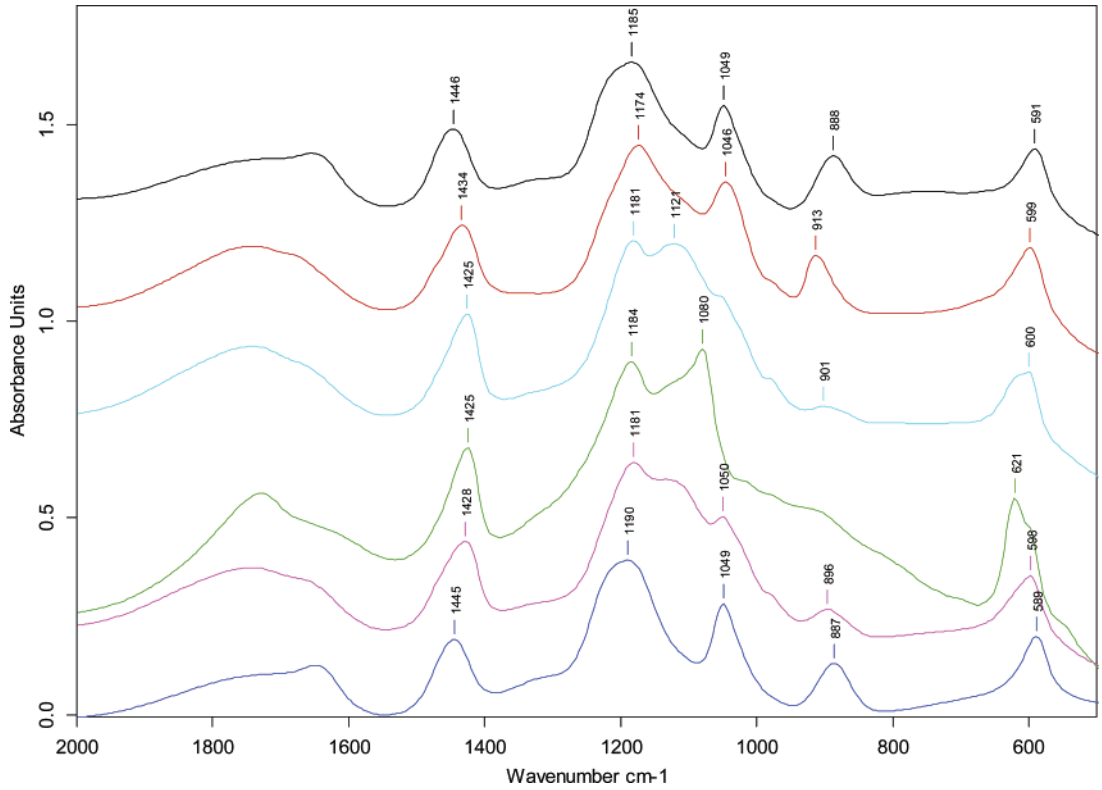

Figure 15. Infrared spectra showing the cooling and warming history of a 35/20 wt % $H_2SO_4/(NH_4)_2SO_4$ sample: blue (279 K) completely liquid sample; purple (214 K) letovicite formation; green (186 K) ice and SAT have formed after cooling to 170 K; light blue (199 K) SAT and ice melted over the range 197 to 199 K; red (224 K) letovicite converts to ammonium bisulfate over the range 210 to 224 K; black (253 K) ammonium bisulfate continuously dissolves until dissolution has completed by 253 K where only liquid remains. Spectra are offset by the following for clarity: blue, −0.15; purple, 0; green, +0.1; light blue, +0.5; red, +0.8; black, +1.05.

case. To demonstrate this, we have selected a point in the region in discrepancy: where we predict the NH_4HSO_4 primary phase field to exist, but the AIM predicts the letovicite primary phase field to exist. The point has the concentration $H_2SO_4/(NH_4)_2SO_4$: 35/20 wt % represented by the red triangle in Figure 14. To examine this point and the differences that would be expected based on our construction of the phase diagram and that predicted by the AIM, it is useful to consider the melting history of a completely frozen sample. In both cases, the sample would begin to melt at or around point C on the diagram. In our picture of the phase diagram (black phase boundaries), upon warming, the liquid concentration will follow the ice/NH_4HSO_4 phase boundary (moving to the right on the diagram) until the point where the red tie line intersects the phase boundary. Then the liquid follows the red tie line until the final melt of NH_4HSO_4 at the red triangle. Therefore, the melting order would be SAT (if it forms), SAH (if it forms), ice, NH_4HSO_4. Conversely, upon warming, the AIM predicts the liquid concentration will follow the letovicite/SAH phase boundary (down and to the left, green phase boundaries) from point C until the blue tie line intersection. Then letovicite will dissolve along the blue tie line until its final dissolution at the red triangle. Thus, the melting order in this model would be ice, SAH, letovicite. The experimental evidence supports our melting history as seen in the green thermogram in Figure 9 and IR spectra in Figure 15. In the DSC sample, SAT formed (rather than the thermodynamically stable SAH), which melts at 197 K, followed by the melting of ice. The letovicite/H_2SO_4 then recrystallizes into NH_4HSO_4 via eq 2, which is completed by 227 K. Then, NH_4HSO_4 continuously melts until the final melt at 251 K. The identity of the solids undergoing phase transitions is confirmed in the IR results (Figure 15). Here, as the sample is cooled letovicite forms first at 214 K as seen by the shift in the NH_4^+ peak from 1445 to 1428 cm^{-1}, the appearance of the peak at 1034 cm^{-1}, and the shift of the SO_4^{2-}/HSO_4^- peak from 589 to 598 cm^{-1} (purple spectrum). Our sample was cooled to 170 K where ice and SAT began to form and completed formation by 185 K (during warming) as indicated by the appearance of the SAT peaks at 1080 and 621 cm^{-1} and the shift in the OH peak at 3600 cm^{-1} (not shown in figure), the increase in the broad ice peak at 918 cm^{-1} and the sharpening of the peak at 1728 cm^{-1} (green spectrum). Over the temperature range 197 to 199 K, the SAT and ice melt leaving only letovicite (light blue spectrum). Upon further warming reaction 2 occurs converting letovicite and H_2SO_4 into NH_4HSO_4 over the range 210 − 224 K as indicated by the diminishment of the letovicite peak at 1121 cm^{-1} and the appearance of the NH_4HSO_4 peak at 913 cm^{-1} (red spectrum). The NH_4HSO_4 continuously dissolves from 224 K to the final dissolution between 251 and 253 K where only liquid remains (black spectrum). More details on peak assignments are given in Beyer and Bothe.[11] Thus, although it is clear letovicite does form at this concentration and appears to form first from our IR experiments, it is a metastable solid in this region and is readily converted to NH_4HSO_4 via reaction 2. Other samples near the NH_4HSO_4/letovicite phase boundary (35−40 wt % H_2SO_4, $[(NH_4)_2SO_4]$ >15 wt %) also formed letovicite first (even though these concentrations are outside the letovicite stability region), which converted to NH_4HSO_4 upon warming. Therefore, we conclude that this region falls in the NH_4HSO_4 stability region as given by our phase boundaries in the phase diagram. Thus, we also conclude the AIM-predicted phase boundary in this region is incorrect.

Summary

We have investigated the water-rich and sulfuric acid-rich regions of the $H_2SO_4/(NH_4)_2SO_4/H_2O$ ternary phase diagram. We have coupled this data with literature data at high temperatures to arrive at the following conclusions:

1. Four invariant points have been determined, two ternary eutectics and two tributary reaction points. The ternary eutectics are ice/letovicite/$(NH_4)_2SO_4$ at 247.6 ± 0.1 K, 5.0−8.8/35.5−37.0 wt % $H_2SO_4/(NH_4)_2SO_4$; ice/SAH/NH_4HSO_4 at 207.2 ± 0.3 K, 35 ± 2/5 ± 1 wt % $H_2SO_4/(NH_4)_2SO_4$. The tributary reaction points are: ice/letovicite/NH_4HSO_4 at 223.8 ± 0.8 K, 29 ± 1/12 ± 1 $H_2SO_4/(NH_4)_2SO_4$; SAH/SAT/NH_4HSO_4 at 218.1 ± 0.8 K, 42 ± 1/4 ± 1 $H_2SO_4/(NH_4)_2SO_4$.

2. We observed that SAT commonly formed outside its stability region, which in this system is very small. Our evidence showed that metastable SAT melted at 195.4 ± 1.0 K and the melt with some letovicite readily recrystallized into ice and ammonium bisulfate.

3. As in the H_2SO_4/H_2O binary system, SAH is difficult to form, and appears to mostly form from the recrystallization of the SAT melt.

4. Sulfuric acid octahydrate (SAO) is not a significant fraction of the solids formed in this system, unlike the $H_2SO_4/HNO_3/H_2O$ system where it is a significant fraction of the solids formed over a large concentration range.[33] We observe transitions in the DSC experiments which we have interpreted to be the melting of SAO, but since the amount of solid is so small, we are not able to confirm the appearance of SAO with IR experiments.

5. Two true binary systems have been determined: ice/letovicite and SAT/ammonium bisulfate. We have clear experimental evidence for the ice/letovicite system, whereas conclusions on the existence of the SAT/NH_4HSO_4 binary system are based on theoretical principles.

6. From our melting point data and that from the literature,[8] we are able to construct the phase diagram with temperature contours for the final melting/dissolution points. We also parametrized our data using first and second-order polynomials and found good agreement with the data.

7. Using the respective fusion enthalpies, we have determined the fraction of the solid phase that is ice and SAT, respectively. As expected, ice is a major fraction of the solid phase in its primary phase region but is also a significant fraction in the letovicite region at low H_2SO_4 concentrations. SAT is a significant fraction of the solid phase even in regions far outside the SAT stability region. However, in these areas it is forming as a metastable solid and decomposes at 195 K.

8. Upon comparison of our melting temperature results and those determined by using the AIM,[18] significant differences occur for concentrations over the entire range studied here. The average (absolute value) of differences is 5.3 K.

9. The AIM model also predicts the ammonium bisulfate/letovicite phase boundary at significantly different concentrations than determined by our study for temperatures below 263 K. Our determination of the ice/ammonium bisulfate/letovicite tributary reaction point is not predicted by AIM. Additionally, we have no evidence for the SAT/NH_4HSO_4/letovicite eutectic predicted by the AIM.

These results have substantial implications for solids that could exist at equilibrium under atmospheric conditions, and the temperatures and conditions at which they will exist. A primary conclusion is the fact that ice and NH_4HSO_4 can coexist at equilibrium, contrary to what is predicted by the AIM. For concentrations in the $(NH_4)_2SO_4$ rich, H_2SO_4 poor regions of

the diagram, ice/NH_4HSO_4 will coexist up to 224 K at which point NH_4HSO_4 will convert to letovicite + H_2SO_4 (aq). A second significant conclusion is the temperature at which liquid can exist at equilibrium, which is heavily dependent on the total composition of the system as given by the phase diagram.

Acknowledgment. We thank Dr. Simon Clegg for many helpful comments on our manuscript. This work was supported by the NSF Atmospheric Chemistry Program (ATM-0304966 and ATM-0442273).

Supporting Information Available: Table 1S contains the experimentally determined melting temperatures for the H_2SO_4/$(NH_4)_2SO_4$/H_2O system used to create Figure 3. This material is available free of charge via the Internet at http://pubs.acs.org.

References and Notes

(1) Mason, B. J. *The Physics of Clouds*; Oxford University Press: New York, 1957; pp 67, 81−82.
(2) Warneck, P. *Chemistry of the Natural Atmosphere*, 2nd ed.; Academic Press: San Diego, 2000; pp 405−428.
(3) Talbot, R. W.; Dibb, J. E.; Loomis, M. B. *Geophys. Res. Lett.* **1998**, *25*, 1367−1370.
(4) Tabazadeh, A.; Toon, O. B. *Geophys. Res. Lett.* **1998**, *25*, 1379−1382.
(5) Martin, S. T. *Geophys. Res. Lett.* **1998**, *25*, 1657−1660.
(6) Seinfeld, J. H.; Pandis, S. N. *Atmospheric Chemistry and Physics*; Wiley: New York, 1998; pp 440−446.
(7) Hu, J. H.; Abbatt, J. P. D. *J. Phys. Chem. A* **1997**, *101*, 871−878.
(8) Silcock, H. L. *Solubilities of Inorganic and Organic Compounds*; Pergamon: Oxford, 1979; Vol. 3.
(9) Tang, I. N. *J. Aerosol Sci.* **1976**, *7*, 361−371.
(10) Brosset, C. *Atmospheric Sulfur Deposition*; Schriner, D. S., Ed.; Ann Arbor Science: Ann Arbor, MI, 1980; pp 145−152.
(11) Beyer, K. D.; Bothe, J. *J. Phys. Chem. A* **2006**, *110*, 7105−7112.
(12) Yao, Y.; Massucci, M.; Clegg, S. L.; Brimblecombe, P. *J. Phys. Chem. A* **1999**, *103*, 3678−3686.
(13) Beyer, K. D.; Hansen, A. R.; Poston, M. *J. Phys. Chem. A* **2003**, *107*, 2025−2032.
(14) Kendall, J.; Landon, M. L. *J. Amer. Chem. Soc.* **1920**, *42*, 2131−2142.
(15) Potemin, C. C. *Vestn. Leningrad. Univ.* **1990**, *2*, 89−92.
(16) Timmermans, J. *The Physico-chemical Constants of Binary Systems in Concentrated Solutions*; Interscience: New York, 1960; pp 619−621.
(17) Linke, W. F. *Solubilities of Inorganic and Metal-Organic Compounds*; American Chemical Society: Washington, DC, 1965; Vol 2, p 755.
(18) Clegg, S. L.; Brimblecombe, P.; Wexler, A. S. *J. Phys. Chem. A* **1998**, *102*, 2137−2154.
(19) Zhang, R.; Wooldridge, P. J.; Abbatt, J. P. D.; Molina, M. J. *J. Phys. Chem.* **1993**, *97*, 7351−7358.
(20) Lide, D.R., Ed.; *CRC Handbook of Chemistry and Physics*, 74th ed.; CRC Press: Boca Raton, FL, 1993; pp 3−208, 351, and 6−58.
(21) Bertie, J. E.; Labbe, H. J.; Whalley, E. *J. Chem. Phys.* **1969**, *50*, 4501.
(22) Pouchert, C. J. *The Aldrich Library of FT-IR Spectra*; Aldrich: Milwaukee, WI, 1997; p 4751.
(23) Miller, F. A; Wilkins, C. H. *Anal. Chem.* **1952**, *24*, 1253−1294.
(24) Damak, M;, Kamoun, M.; Daoud, A.; Romain, F.; Lautie, A.; Novak, A. *J. Mol. Struct.* **1985**, *130*, 245−254.
(25) Schubnell, M. *J. Therm. Anal. Calorim.* **2000**, *61*, 91.
(26) Czizo, D. J.; Abbatt, J. P. D. *J. Geophys. Res.* **1999**, *104*, 13781−13790.
(27) Bertram, A. K.; Koop, T.; Molina, L. T.; Molina, M. J. *J. Phys. Chem. A* **2000**, *104*, 584−588.
(28) Kamiyoshi, K. *J. Chem. Phys.* **1957**, *26*, 218−219.
(29) Jain, Y. S.; Bist, H. D.; Upreti, G. C. *Chem. Phys. Lett.* **1973**, *22*, 572−575.
(30) Fortin, T. J.; Shilling, J. E.; Tolbert, M. A. *J. Geophys. Res.* **2002**, *107*, DOI 10.1029/2001JD000677.
(31) Atkins, P.; de Paula, J. *Physical Chemistry*, 8th ed.; W. H. Freeman: New York, 2006; pp 189−191
(32) Ehlers, E. G. *The Interpretation of Geological Phase Diagrams*; Dover: Mineola, NY, 1972; p 42.
(33) Beyer, K. D.; Hansen, A. R.; Raddatz, N. *J. Phys. Chem. A* **2004**, *108*, 770−780.
(34) Zeleznik, F. J. *J. Phys. Chem. Ref. Data* **1991**, *20*, 1157.
(35) Windholz, M., Budavari, S., Eds.; *The Merck Index* 10th ed.; Merck & Co., Inc.: Rahway, NJ, 1983; p 586.